Results in Engineering 30 (2026) 110058

Contents lists available at ScienceDirect

Results in Engineering

journal homepage: www.sciencedirect.com/journal/results-in-engineering

Research paper

Meniscal extracellular matrix remodelling caused by injuries and degeneration

Maddalena Bracchi [a], Riccardo Campanile [a], Marco Crippa [a,b], Mario Mauri [a], Valeria Cassina [a], Francesco Mantegazza [a], Francesco Nicotra [a], Judith Waldner [a,b], Giovanni Zatti [a,b], Marco Bigoni [a,b,c], Marco Turati [a,b,*], Laura Russo [a,d,e,**]

[a] School of Medicine and Surgery, Università degli Studi di Milano-Bicocca, Monza, Italy
[b] Orthopedic Department, Fondazione IRCCS San Gerardo dei Tintori, Monza, Italy
[c] Department of Orthopedic Surgery, Policlinico San Pietro, Ponte San Pietro, Italy
[d] Fondazione IRCCS San Gerardo dei Tintori, Monza, Italy
[e] CURAM Research Ireland Centre for Medical Devices, University of Galway, Galway, Ireland

ARTICLE INFO

Keywords:
Meniscus
ECM
Collagen
GAGs
Knee

ABSTRACT

The characterization of meniscal extracellular matrix (ECM) is fundamental for tissue engineering to design a functional substitute. However, most of the available data come from animal studies. The meniscus has a complex ECM, characterized by a specific orientation of collagen fibres related to its function. In this work, both pediatric and adult meniscal tissues were examined from morphological, biochemical, and mechanical perspectives to identify the characteristics of physiological tissue and the changes caused by injuries and degeneration. Additionally, a comparison was performed between menisci from patients with normal and valgus knees to observe ECM remodeling associated with altered biomechanics. Obtained results indicatet that, with both aging and pathology, collagen and glycosaminoglycans (GAG) content decreased, while mucins increased. These changes were accompanied by alterations in tissue structure at both the macroscopic and nanoscale levels, including less organized collagen networks and thicker, more fibrotic fibres. Correspondingly, the elastic modulus decreased with age, reflecting a loss of tissue mechanical integrity. The various results from the morphological, biochemical, and mechanical analyses were then correlated in a qualitative and descriptive manner to provide a comprehensive impression of tissue organization and remodelling. Finally, the obtained results were compared with data available in the literature to highlight similarities and differences between humans of various ages and animal models.

1. Introduction

The extracellular matrix (ECM) is a non-cellular complex polymer network that mirrors the biochemical and mechanical properties of a tissue and undergoes continuous remodelling, especially during pathological conditions [1]. In tissue engineering, a meniscal scaffold should mimic the biomolecular features and composition of the native tissue to achieve a functional substitute.

Recently, increasing attention has been directed to understand the role of the ECM as a key regulator of cell fate modulation. The biochemical and physical properties of ECM are known today to be involved in the regulation of specific cell behaviour essential for successful regulation of tissue homeostasis and tissue regeneration. The biochemical composition and the structural organization of the ECM provide instructive signals that guide cell fate influencing tissue functionalities. As consequence, the reproduction of key ECM features in engineered biomaterials and scaffolds represent a critical requirement to control tissue integration and functional response.

In this context, the detailed characterization of physiological and pathological meniscal tissue is fundamental to correctly determine the biochemical and mechanical changes during ECM remodelling, which is crucial for designing an effective replacement for regenerative medicine applications [2,3].

Meniscal tears are among the most common intra- articular injuries

* Corresponding author at: Orthopedic Department, Fondazione IRCCS San Gerardo dei Tintori, Monza, Italy.
** Corresponding author at: School of Medicine and Surgery, Università degli Studi di Milano-Bicocca, Monza, Italy.
E-mail addresses: marco.turati@unimib.it (M. Turati), laura.russo@unimib.it (L. Russo).

https://doi.org/10.1016/j.rineng.2026.110058
Received 25 November 2025; Received in revised form 15 February 2026; Accepted 11 March 2026
Available online 14 March 2026

of the knee and can lead to significant pain and functional impairment [4]. The medial and lateral menisci are fibrocartilaginous structures located within the knee joint, between the femoral condyles and the tibial plateau. Their primary functions include load distribution, facilitation of joint rotation, and stabilization of translational movements [5]. By increasing the contact surface area between the femur and tibia, the menisci play a crucial role in evenly distributing the load transmitted from the femur, thereby reducing stress on the articular cartilage [6]. These mechanical properties are given by their cellular, biochemical and structural composition [7]: their extracellular matrix (ECM) is highly hydrated (70–80 % water); in the remaining portion, collagen (50–75 %), which is responsible of tensile strength, glycosaminoglycans (GAGs, 15–30 %), DNA (2 %), adhesion glycoproteins (<1 %) and elastin (<1 %) are found [8,9]. These data might vary depending on age, injuries and other pathological conditions [10,11], but only limited data are available on human tissues due to the fact that most of the knowledge on menisci comes from animal experiments [11]. The distribution of collagen fibres in the meniscus is highly anisotropic, and three distinct layers can be distinguished: a superficial fibril network which covers femur and tibia articulating surfaces, a lamellar layer radially oriented and a central zone with circumferential fibres [12,13]. Taking the triangular-shaped cross section of the meniscus, three zones can be distinguished from the outside to the inside:

- Red-Red zone (R-R): vascularized, mainly type I collagen, higher mechanical properties and with fibroblast-like cells;
- Red-White zone (R-W): partially vascularized, with intermediate properties;
- White-White zone (W-W): non- vascularized (nutrition depends on synovial fluid diffusion), mainly type II collagen, smoother and with chondrocyte-like cells [5,14].

From the biomechanical point of view, human and animal meniscal tissues have been characterized in several studies. The ovine model is considered the most similar to human tissue in terms of stiffness, compression and residual force, but also vascularity and collagen structure [15,16]. However, Sweigart et al. compared the biomechanical properties of canine, bovine, baboon, porcine, lapine and human menisci, and concluded that animal models are not entirely representative of human meniscus [17]. Histological studies were also performed on human and animal menisci to determine the ECM composition (Table 1). Notably, Sandmann et al. emphasized that no animal model fully replicates the histological and structural characteristics of the human [16]. To overcome this limitation, in this work a multiscale characterization of human meniscal tissue has been evaluated considering the effect of aging on the composition of meniscal ECM and the first comparison between healthy and valgus-aligned menisci.

Meniscal tissue has a very limited healing capacity due to its poor vascularization. Despite this, injuries are quite common and can be classified as either traumatic or degenerative. Traumatic lesions occur in patients with previously healthy joints when excessive forces are applied to the articulation; in contrast, degenerative lesions are frequently associated with aging and the presence or onset of osteoarthritic disease [23,24]. During the degenerative process of the knee, macroscopic and microscopic variations in the ECM can be observed [7]. Understanding these changes is crucial for the development of meniscal substitutes in regenerative medicine, where the physiological characteristics of native tissue must be mimicked. In this study, histological, morphological and biomechanical properties of menisci from paediatric and adult patients with different pathologies were investigated to discover the variations between physiological and pathological tissues. Additionally, a comparison was made between normal and valgus knees to evaluate differences in the behaviour of medial and lateral menisci.

2. Materials and methods

2.1. Samples collection

Human menisci were obtained from patients undergoing arthroscopic meniscectomy, occasionally in conjunction with Anterior Cruciate Ligament reconstruction, or total knee arthroplasty at the Orthopaedic and Traumatology Unit of IRCCS San Gerardo dei Tintori Hospital, Monza. The material collected was discarded tissue, which would have been disposed of at the end of the surgical procedures. Arthroscopic en bloc meniscectomy technique was performed only in patients with a significant traumatic meniscal lesion (e.g., peripheric bucket- handle tears) who refused to be treated with meniscal repair for personal and specific reasons (e.g., impossibility to follow an adequate follow-up and rehabilitation protocol). All patients were informed about the study protocol and provided written informed consent for the use of their tissue samples. The study was conducted in accordance with the Declaration of Helsinki, and the use of anonymized residual surgical tissue samples was approved by the local institutional ethical committee.

2.1.1. Inclusion criteria

- Paediatric or adult patients with meniscal injuries treated with arthroscopic meniscectomy surgery (performed using the en bloc technique).
- Paediatric or adult patients with anterior cruciate ligament injury requiring reconstructive surgery and concomitant meniscal injury necessitating meniscectomy
- Adult patients with severe gonarthrosis requiring total knee arthroplasty surgery

2.1.2. Exclusion criteria

- Meniscal tears treated by arthroscopic meniscectomy using shavers instead of the en bloc technique.
- Small meniscal tears where obtaining an adequate sample for analysis was not possible.
- Meniscal lesions where it was not possible to definitively determine the originating portion of the meniscus.
- Presence of arthritis or chronic inflammatory diseases.
- History of intra-articular drug injections.

After removal, the meniscal pieces were immediately placed in sterile tubes containing 10 mL of 0.9 % NaCl physiological solution, stored in a container with ice and transferred to the laboratory. There,

Table 1
Histological studies found in literature on human and animal meniscal ECM.

Meniscal tissue	Masson Trichrome	Alcian Blue	Safranin - Fast Green	Van Gieson Trichrome	Haematoxilin - Eosin	References
Human		x	x		x	[11,15,16,18]
Bovine	x		x		x	[16,19]
Ovine			x		x	[15,16]
Pig	x	x	x		x	[16,20]
Horse		x	x	x	x	[21]
Rabbit			x		x	[15,22]

the samples were washed twice with 0.9 % NaCl physiological solution and then stored at −80 °C until further use.

2.2. Histological analysis

Samples stored at −80 °C were gradually defrosted by transferring them to −20 °C; after 24 h, they were washed with 0.9 % NaCl physiological solution, fixed in 10 % formalin for 1 h and washed twice more with 0.9 % NaCl physiological solution. The meniscal pieces were then embedded in tissue freezing medium, frozen for 1 h and sectioned with a cryostat (Leica CM 1520, Cornegliano Laudense, Lodi, Italy) to obtain 5 μm thick coronal sections.

The slices were mounted on microscope slides (VWR® SuperFrost® Plus, Milano, Italy) and stained with Haematoxylin-Eosin (Bio-Optica, Milano, Italy) and Van Gieson (Bio-Optica, Milano, Italy) to evaluate the cell morphology and distribution and to have a general overview of tissue organization, Masson's trichrome (Bio-Optica, Milano, Italy) to observe the collagen content and distribution, Alcian blue pH 2.5 (Bio-Optica, Milano, Italy) for the proteoglycans distribution and mucoid degeneration and Safranin – Fast green (Thermo Scientific) to highlight the accumulation of acidophil molecular complexes (proteoglycans and glycosaminoglycans). In Table 2 the characteristics of each stain and the corresponding ECM colours observed after staining are summarized.

The slides were then observed at 10X magnification to compare different patients and 20X magnification to see the differences between Red-Red and White-White zones with an inverted microscope (Zeiss Axio Observer / Cell Observer) and analysed with Zeiss Zen lite. The staining quantification was performed using Fiji ImageJ with the colour deconvolution plugin, and the percentage of each coloration was determined using Equation 1. To minimize potential variability, section thickness was kept consistent across all samples, the same staining kit was used for all sections to avoid batch effects, and identical threshold settings were applied in the software for all quantifications.

$$Stain\ percentage = \frac{Pixels_{stain}}{Total\ Pixels_{sample}} * 100$$

Equation 1 formula used for stains quantification, where $Pixels_{Stain}$ represents the number of the pixels coloured with the respective stain, and Total $Pixels_{sample}$ corresponds to the number of pixels in the meniscal sample before colour deconvolution.

For Masson Trichrome, Alcian Blue pH 2.5, and Haematoxylin-Eosin, pre-inserted vectors were utilized for quantification. However, for Safranin-Fast green and Van Gieson, values were extracted from the regions of interest (ROI) in the images and kept consistent for each stain. A 100 % stacked column graph was then generated for each staining using Origin(Pro), Version 2022 (OriginLab Corporation, Northampton, MA, USA).

2.3. Scanning electron microscopy (SEM)

The morphology of paediatric and adult meniscal tissue was observed with SEM analysis. The collected meniscal tissue was washed three times with demineralized water, frozen at −80 °C for 48 h and freeze-dried with Vacuum Freeze Dryer (Boyikang Laboratory Instruments Inc, Beijing, China) for 24 h at $T = -50$ °C and pressure below 15 Pa. Then, they were put on aluminium supports and covered with a gold coating to make them conductive.

Finally, samples were observed with SEM (Zeiss Gemini 500 GrbH scanning electron microscope, Jena, Germany) at 300X and 1000X magnifications and the collected images were analysed with an image analysis software (Fiji ImageJ). A comparison between the Red-Red zone and White-White zone from paediatric and adult patients was performed to assess differences in surface morphology and microstructural organization. SEM images were acquired at standardized magnifications, and representative fields were analysed qualitatively for fibre alignment, porosity, and surface texture. Fibre diameters and pore area were semi-quantitatively measured using Fiji ImageJ to support the morphological observations.

Table 2
Summary of stain characteristics and resulting ECM colours according to manufacturer datasheets.

Staining	Stained ECM components	Colours
Haematoxylin-Eosin	Cytoplasm, collagen, ECM	Red
	Nuclei	Blue
Van Gieson	Collagen fibres	Red
	Nuclei	Black
Masson's trichrome	Collagen	Blue
	Cytoplasm	Red
Alcian blue pH 2.5	Acidic GAGs	Blue
	Mucins	Purple
Safranin – Fast green	Proteoglycans, cartilage	Red
	Ligamentous tissue, ECM	Green

2.4. Quantitative imaging (QI) mode AFM measurements

The nanoscale surface morphology and mechanical properties of dried meniscal tissue were evaluated using Quantitative Imaging (QI) mode on a NanoWizard 4XP Atomic Force Microscope (AFM, JPK Instruments, Bruker). The Quantitative Imaging (QI) is related to the specific force-distance acquisition mode of the AFM instrument. Even if this mode generates high-resolution quantitative datasets of Young's Modulus, the textual description of these maps in this study is maintained as qualitative to facilitate the spatial correlation between nanoscale architecture and mechanical response. In this mode, a complete force–distance curve is recorded at each pixel, allowing for high-resolution mapping of both topography and mechanical characteristics (Young's Modulus, YM) [25] while minimizing lateral forces during scanning.

Sample slices were prepared as previously described; however, in this case, 30 μm-thick coronal sections were obtained. These sections were rinsed with deionized water to remove residual debris and then left to air dry at room temperature. Once fully dried, they were mounted on the AFM stage for analysis. Measurements were carried out in air using a RTESP (Bruker, AFM probes) cantilever with a nominal spring constant of 30 N/m. Nevertheless, the spring constant was estimated by contact-free calibration methods before each experiment [26,27]. Indentation was performed with a maximum applied force of 60 nN and the approach/retract velocity was set to 120 μm/s.

Force–distance curves were acquired across a scanned area of 2.5 × 2.5 μm^2 with 512 × 512 points and they were used to extract quantitative tissue stiffness by fitting them with Hertz-Sneddon model [28]. Pairwise comparisons between the datasets of interest were performed using the Mann–Whitney test, which is a non-parametric test designed to evaluate differences between two independent samples. This test does not assume normal distribution and is appropriate for ordinal or non-normally distributed continuous data. Statistical analyses were performed using non-parametric tests due to the non-normal distribution of AFM-derived mechanical data. Differences between conditions were evaluated through pairwise comparisons, applying the Mann–Whitney U test to each pair of datasets of interest. Each comparison therefore involved only two independent samples at a time. All analyses were performed using GraphPad Prism (GraphPad Software, San Diego, CA, USA). Statistical significance was defined as $p < 0.05$.

2.5. Compression test

The global mechanical properties of meniscal tissue were evaluated by compression test using a Texture Analyzer (Stable Micro Systems, Godalming, United Kingdom) equipped with a 2 mm cylindrical probe. Meniscal cross-sections, 2.5 mm thick, were prepared with a scalpel and hydrated in PBS pH 7.4 at room temperature for 3 h. Compression was

performed until 40 % deformation with pre- and post-test speeds of 10 mm/min, a test speed of 0.5 mm/min, and a trigger force of 0.05 N. Stress–strain curves were obtained in triplicate for each sample, and R–R and W–W zones were analysed to calculate YM. Statistical analysis was conducted in OriginPro 2022b For the compression tests, medial and lateral R-R and W-W zones from patients P6, P7, and P8 were compared using one-way ANOVA, followed by Tukey's post-hoc test for multiple comparisons. Prior to performing ANOVA, the normality of each group was assessed using the Shapiro-Wilk test. Differences were considered statistically significant at $p < 0.05$.

3. Results

3.1. Samples collection

A total of eight patients were included in this study: two of them belong to the paediatric group (age < 18 years), the other six to the adult group (age ≥ 18 years). The mean age in the paediatric group was 14.5 $\pm$ 0.5 years and 65.2 $\pm$ 14.2 years in the adult group; the characteristics of the population examined in this study are shown in Table 3.

3.2. Histological analysis

The results of histological analysis on meniscal tissue of patients are shown in Fig. 1. Due to the high heterogeneity of meniscal tissue, the central region of the meniscus was selected for characterization. In the first column, Masson's Trichrome staining highlighted a ligament-like outer zone, predominantly composed of collagen fibres, which appear blue. In contrast, the inner zone exhibited a more cartilage-like structure, rich in negatively charged proteoglycans, stained red with Safranin-Fast Green (second column, Fig. 1). GAGs were uniformly distributed throughout the section, appearing blue with Alcian Blue (third column). Overall, cellularity was low: elongated fibroblast-like cells were observed in the R-R zone, whereas rounded chondrocyte-like cells became more frequent toward the W-W zone, with the outer region showing slightly higher cell density. Cellularity was visualized using Haematoxylin-Eosin and Van Gieson stains, presented in the fourth and fifth columns, respectively.

Table 3
Index of patients used for meniscal tissue characterization, ACL indicates Anterior Cruciate Ligament, TKA indicates Total Knee Arthroplasty.

Patient	Age	Sex	Knee	Portion	Alignment	Intraoperative findings
P1	14	Male	Left	Lateral	Normal	Traumatic lateral meniscal tear associated with a complete ACL tear
P2	15	Male	Left	Medial	Normal	Isolated traumatic medial meniscal tear
P3	25	Male	Left	Lateral	Normal	Traumatic lateral meniscal tear associated with a complete ACL tear
P4	48	Female	Right	Medial	Normal	Isolated traumatic meniscal injury
P5	77	Female	Right	Lateral	Normal	Macroscopic good quality of lateral meniscus in patient treated with TKA for osteoarthritis
P6	82	Female	Left	Medial + Lateral	Valgus	Macroscopic good quality of lateral and medial meniscus in patient treated with TKA for osteoarthritis
P7	56	Female	Right	Medial + Lateral	Valgus	Macroscopic good quality of medial and lateral meniscus in patient treated with TKA for osteoarthritis. in a valgus knee
P8	63	Female	Left	Medial + Lateral	Normal	Macroscopic good quality of medial and lateral meniscus in patient treated with TKA for osteoarthritis

In Fig. 2, stain percentages and respective percentage stacked column graphs are pictured. These percentages were calculated using the colour deconvolution function on stained images. In Masson's trichrome, the red stain represents the cytoplasm of cells, while the blue stain indicates collagen content (Fig. 2A). Higher collagen percentages were observed in P1, P2, and P4, with values of 64 %, 60 %, and 60 %, respectively, whereas the lowest levels were found in P5 and P7 lateral (26 % and 24 %). In Safranin–Fast Green, purple indicates proteoglycan content, and green represents the fibrous ECM (Fig. 2B). Proteoglycans were more abundant in P2 and P5 (50 % and 70 %), although their percentage was reduced in P4, P6 lateral, P7 lateral and P8 lateral, with values of 27 %, 23 %, 28 % and 26 %, respectively. In Alcian Blue, blue denotes GAGs content, while purple highlights mucins (Fig. 2C). In this case, GAGs were more present in P1, P2, P6 medial, P6 lateral and P7 lateral (93 %, 79 %, 84 %, 80 % and 79 %), although in P4 and P5 mucins were more abundant (64 % and 67 %). In Haematoxylin–Eosin, blue marks the cell nuclei, red represents both the cytoplasm and protein structures (Fig. 2D). All patients exhibited low cellularity, with values ranging from 10 % to 17 %. Lastly, in Van Gieson, black indicates cell nuclei, while red marks the cytoplasm and fibres (Fig. 2E). Similarly, the presence of cell nuclei was reduced, with values ranging from 2 % to 14 %. Greater variability was observed in this case, with the lowest values in P5 and P7 medial, and the highest in P2. At this point, two comparisons were performed: P1-P5 samples were used to compare physiological-paediatric and pathological-adult tissues, P6-P8 to investigate the differences between medial and lateral menisci in conditions of normal and valgus knee.

3.2.1. Comparison between paediatric and adult tissues

In adult patients, collagen and GAG content was noticeably reduced, while mucin levels increased, reflecting tissue degeneration, particularly in P5. In contrast, the two paediatric patients showed similar percentages of collagen and GAGs (Figures S1 and S3, Supplementary Material). Proteoglycan distribution varied widely among all patients (Figure S2, Supplementary Material). Notably, in P1 and P2, proteoglycans were concentrated in the inner zone and were less abundant in the outer region, whereas in adults, their distribution appeared more random (Figure S2, Supplementary Material). Cell distribution was consistent across all samples, with elongated cells in the outer zone and rounded cells in the inner zone (Figures S4 and S5, Supplementary Material). Overall, although cellularity was relatively low, a slight decline in cell numbers was observed with advancing meniscal degeneration.

3.2.2. Comparison between lateral and medial menisci in normal and valgus knee

In P8, the lateral meniscus showed a slightly higher collagen content compared to the medial meniscus. A similar trend was observed in P6 lateral and P7 medial menisci, which exhibited less damage than their lateral counterparts (Figure S6, Supplementary Material). Regarding GAG distribution, no significant differences were found between the medial and lateral menisci of P7 and P8. In contrast, P6 showed lower GAG content and higher mucin levels in the lateral meniscus (Figure S8, Supplementary Material). Proteoglycan content was consistently lower

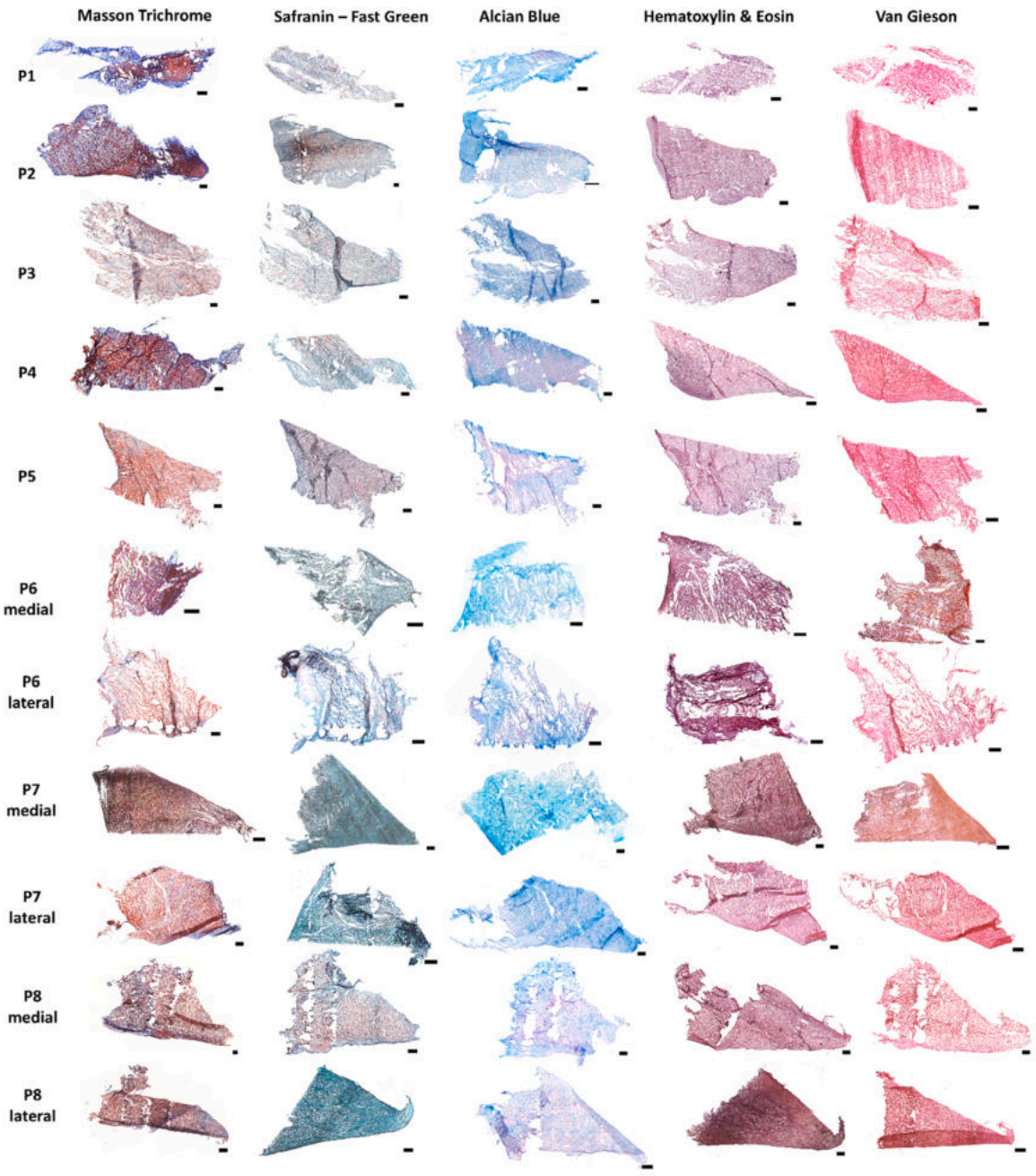

Fig. 1. Histological characterization performed on 5 μm slices of meniscal tissue from P1-P8 patients, 10X magnification, scale bar: 500 μm.

in lateral menisci compared to medial ones, regardless of knee alignment (Figure S7, Supplementary Material). In normal knees, the medial meniscus is more subjected to damage due to its higher congruency and attachment to the medial collateral ligament. In valgus knees, altered stress distribution increases loading on the lateral meniscus, making it more susceptible to degeneration. Overall, cellularity was similar across all samples (Figures S9 and S10, Supplementary Material).

3.3. Morphological analysis

Morphological characterization of meniscal tissue was conducted to examine its key structural features and identify changes associated with pathology. Given the high heterogeneity of this tissue, the central region was selected for analysis. Initial observations at low magnification allowed assessment of the overall collagen fibre orientation. The collagen architecture within the meniscus is illustrated in Fig. 3: at the edges in contact with the femoral and tibial articulating surfaces, fibres are radially oriented, whereas the central region exhibits a porous structure formed by sections of circumferential fibres. This architectural pattern is observed in both paediatric and adult tissues.

Menisci were then examined at higher magnifications to investigate structural differences associated with various pathologies and injuries. Comparing pediatric and adult tissues (Fig. 4), P1 and P2 displayed regular pores with thinner, smoother fibres, and similar porosity in the R-R and W-W zones. With increasing age, pores became less regular and fibres thicker and more wrinkled, reflecting the accumulation of fibrotic tissue, particularly in the W–W zone, which appeared less porous.

A second comparison was performed between patients with normal and valgus knee configurations, with results shown in Fig. 5. Overall porosity was similar across all samples: the R-R zone appeared more porous than the W-W zone, which exhibited a more irregular collagen fibre distribution. In the R-R zone, collagen fibres in P6 lateral, P7

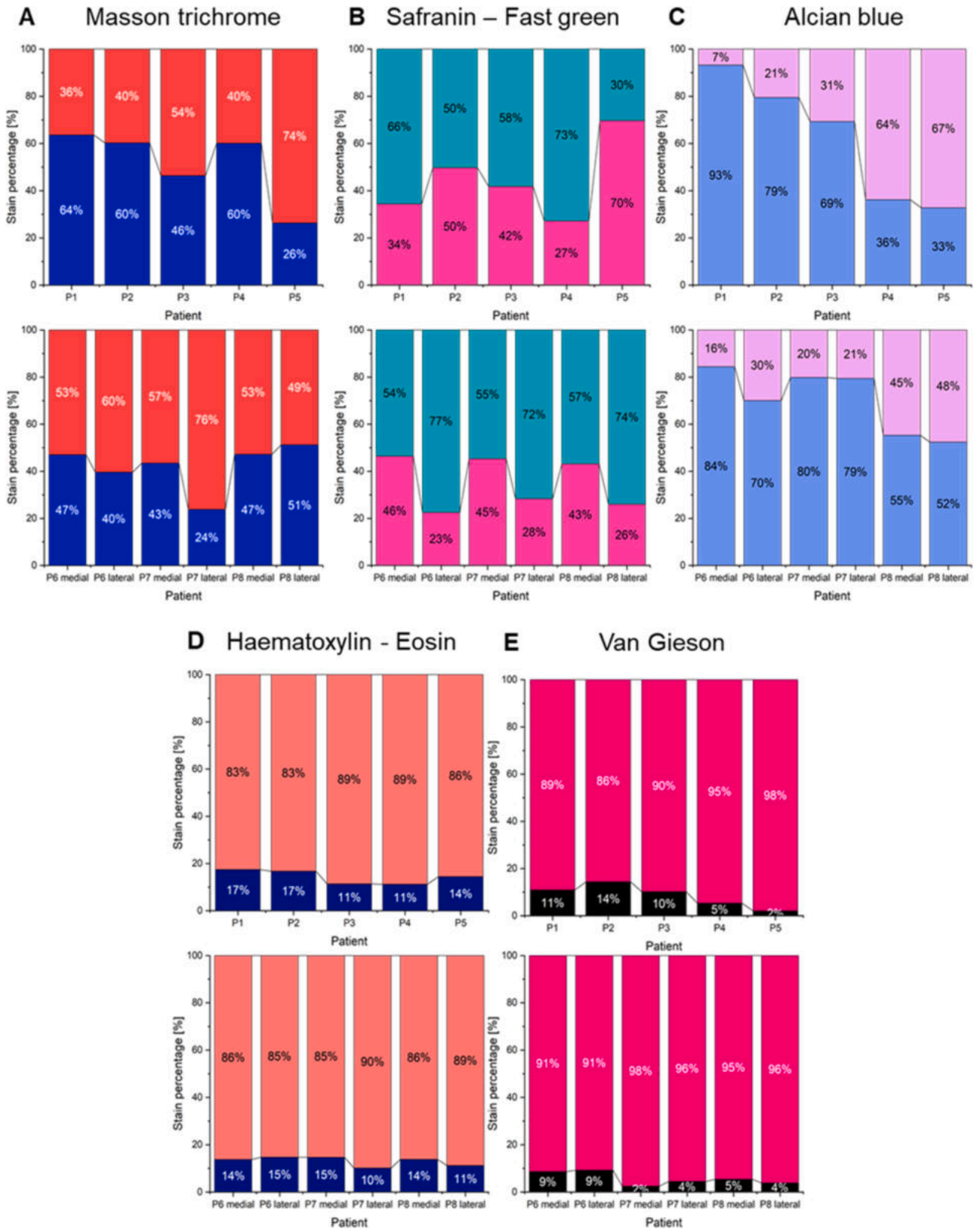

Fig. 2. Percentage stacked column graphs generated from objective digital quantification of histological stains. Specifically: (A) blue represents collagen content stained with Masson, and red represents cytoplasmic content; (B) pink indicates positive Safranin staining, and green shows the Fast green counterstain; (C) blue represents GAG content stained with Alcian Blue, and purple corresponds to mucin stain; (D) blue indicates nuclei stained with Haematoxylin, and pink represents Eosin counterstain; (E) black represents nuclei, and red indicates collagen stained with Van Gieson.

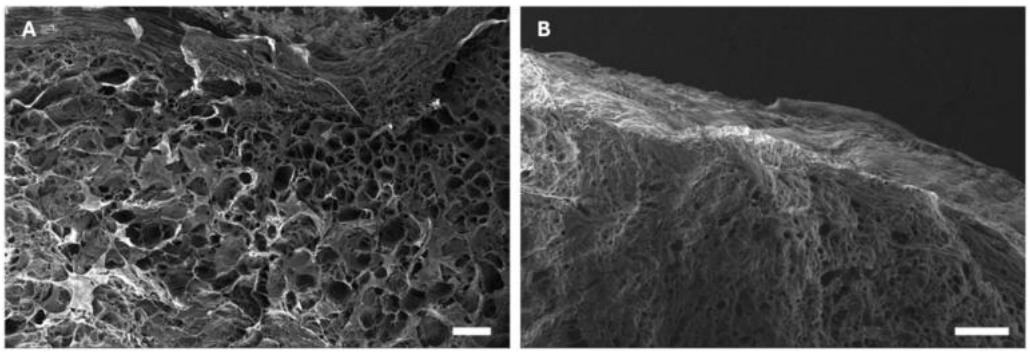

Fig. 3. SEM images of P1 (A) and P5 (B) sections, scale bar: 200 μm.

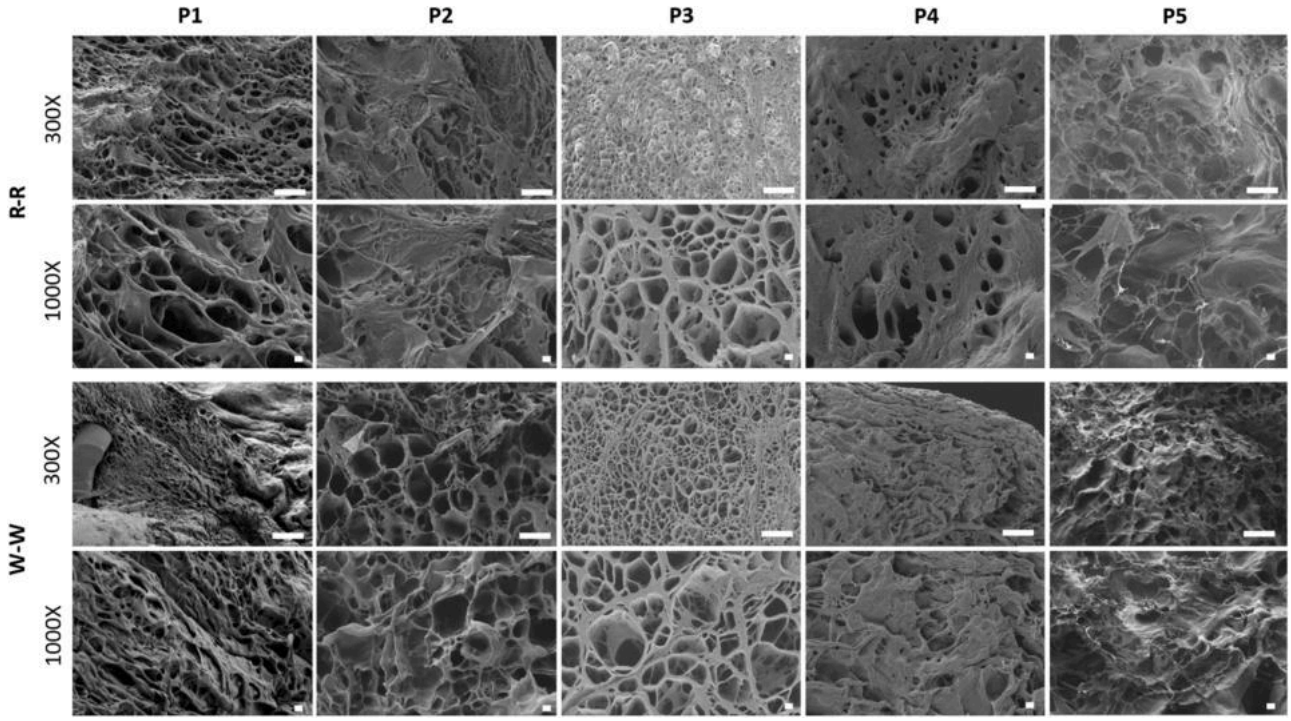

Fig. 4. SEM images of R-R and W-W zones of P1-P5 at 300X and 1000X magnifications. Scale bars: 100 μm (300X) and 10 μm (1000X).

lateral, and P8 medial were more frayed compared to P6 medial, P7 medial, and P8 lateral, where fibres appeared less damaged.

Fibre diameter and pore size were quantified using Fiji ImageJ, and the results are summarized in Table 4. The reported measurements of fibre diameter and pore area are presented for descriptive purposes to illustrate inter-patient variability and trends, and they were not subjected to inferential statistical analysis. The increase of the observed fibre diameter (exceeding 20 μm in older patients) and the less regular pore structure in adult samples are considered as morphological indicators of tissue fibrosis and loss of structural integrity associated with aging and degeneration.

Regarding fibre diameter, smaller values were observed in paediatric patients. Diameter then increased in P3 and continued to rise with age, reaching values above 20 μm in patients older than 40 years. When comparing valgus and normal knees, patients with valgus alignment tended to exhibit larger fibre diameters in the medial meniscus; however, in P8 the lowest diameter was observed in the lateral meniscus. These observations indicate qualitative trends rather than statistically supported differences. Overall, fibre diameter appeared to increase with both ageing and tissue degeneration, likely reflecting the presence of fibrotic tissue.

In terms of pore area, paediatric patients showed the highest mean values, followed by intermediate values in P3, and similar values across the remaining adult patients. Notably, standard deviations were larger in adult samples and in some cases approached the mean values, indicating greater variability in pore size among adult patients.

3.4. Quantitative imaging (QI) mode AFM measurements

The surface morphology and mechanical properties of meniscal tissues from patients P6, P7, and P8 were assessed using QI mode AFM. Only patients with both medial and lateral menisci available were included, as the goal was to evaluate morphological and mechanical changes associated with valgus knee alignment compared to normal knees. The resulting maps of YM and contact point (cp), together with Alcian Blue-stained and SEM images, are presented below. YM maps provide nanoscale insights into tissue organization through stiffness variations, while cp maps reveal localized surface morphology. Comparisons between YM, Alcian Blue, and SEM images were qualitative and descriptive, intended to provide a visual impression of tissue organization.

At the microscale, the medial meniscus from patient P6 (Fig. 6)

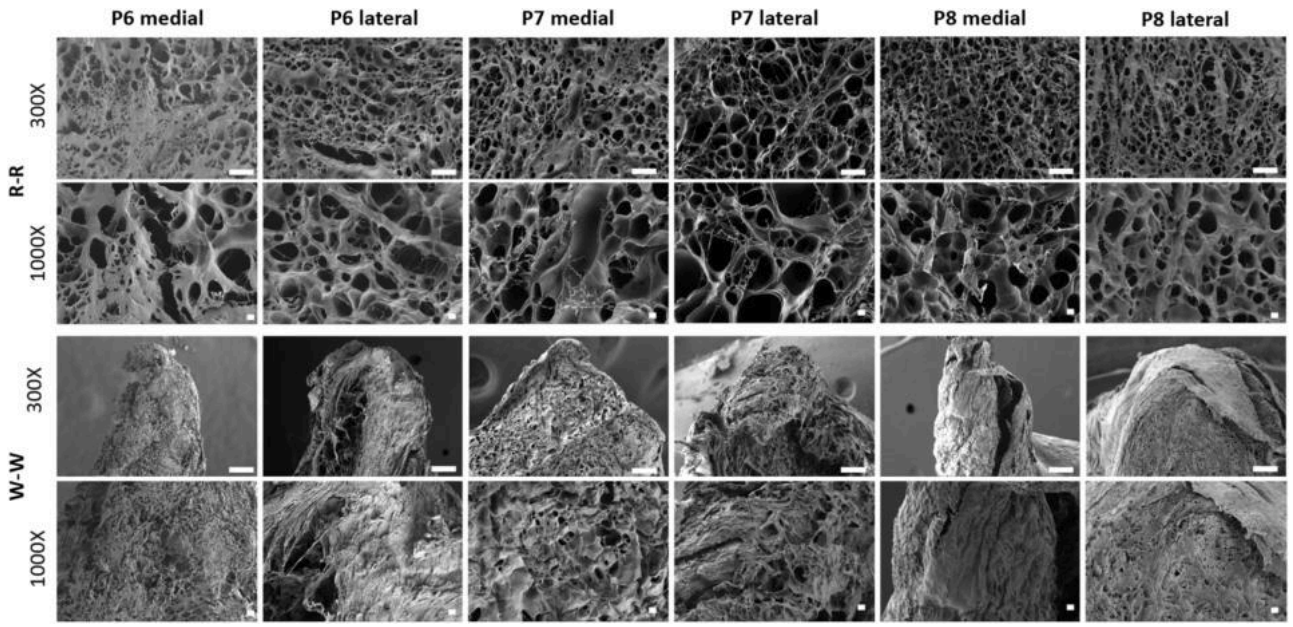

Fig. 5. SEM images of R-R and W-W zones of P6-P8 at 300X and 1000X magnifications. Scale bars: 100 μm (300X) and 10 μm (1000X).

Table 4
fibres diameter and pore area obtained from measures on SEM images; data are expressed as mean ± SD.

Patient	Fibres diameter [μm]	Pore area [μm^2]
P1	6.78 ± 0.84	980 ± 327
P2	6.60 ± 1.03	774 ± 486
P3	11.95 ± 1.57	445 ± 324
P4	25.21 ± 5.49	213 ± 133
P5	20.16 ± 3.20	250 ± 103
P6 medial	31.35 ± 7.46	300 ± 294
P6 lateral	28.71 ± 4.20	333 ± 288
P7 medial	23.80 ± 4.03	252 ± 150
P7 lateral	22.21 ± 3.16	230 ± 121
P8 medial	27.51 ± 5.23	219 ± 220
P8 lateral	28.11 ± 2.97	216 ± 108

displayed a porous matrix, particularly in the R-R zone, which contained larger pores. GAGs were predominant in this region, whereas mucins were more abundant in the inner zone (Fig. 6, Alcian Blue images). At the nanoscale, AFM revealed an amorphous structure in the outer region of the ECM, while the inner region appeared more porous; stiffness, however, was relatively homogeneous (Fig. 6, cp and YM maps).

A similar external architecture was observed in the lateral meniscus of P6 (Fig. 7). In contrast, the W-W zone exhibited greater heterogeneity, featuring a mixture of fibrillar and amorphous regions (Fig. 7, cp and YM maps). The fibrillar structures, measured to be approximately 20–30 μm in diameter using Fiji ImageJ with the scale bar calibrated the image, likely contributed to tissue aggregation. Regions with increased agglomeration were also noted. This dual composition was also observed in the SEM images, where both organized fibrils and less structured areas were clearly visible. The proportions of GAGs and mucins were comparable in both the R-R and W-W zones (Fig. 7 Alcian blue images); however, the ECM appeared more porous externally, while in the W-W zone was more compact and fibrous (Fig. 7 SEM images). In the medial meniscus of patient P7, a porous architecture was microscopically observed in both R-R and W–W zones, which also had a similar GAGs and mucins distribution (Fig. 8 Alcian blue images). In particular, mucins were less abundant compared to P6 lateral, with a

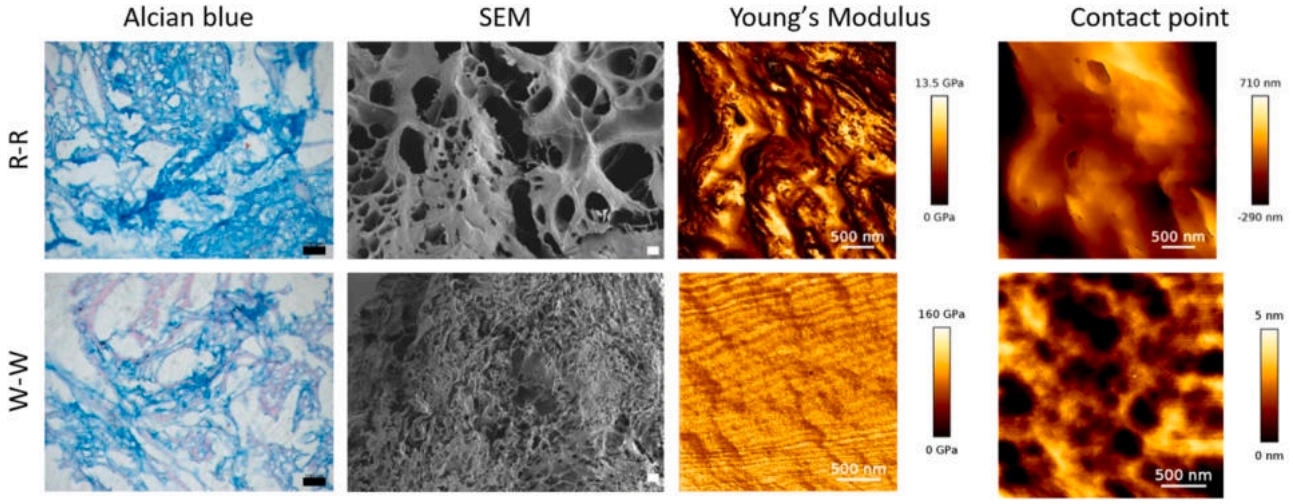

Fig. 6. Alcian blue staining, SEM and AFM images of YM and contact point acquired on P6 medial meniscal tissue. Scale bars: 100 μm for Alcian blue images, 10 μm for SEM images, 500 nm for cp and YM images.

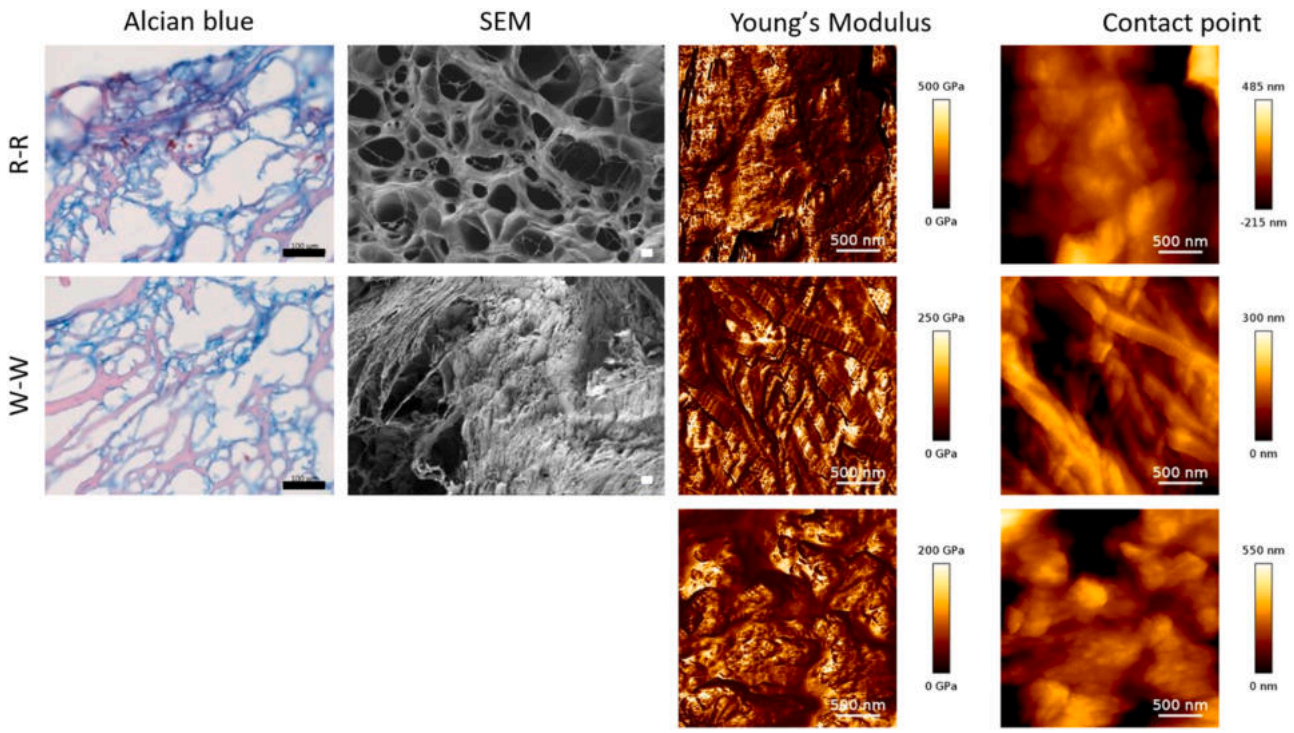

Fig. 7. Alcian blue staining, SEM and AFM images of YM and contact point acquired on P6 lateral meniscal tissue. For W-W zone, two images were acquired due to the heterogeneous compostion of the ECM in this portion. Scale bars: 100 μm for Alcian blue images, 10 μm for SEM images, 500 nm for cp and YM images.

distribution pattern more closely resembling that of the P6 medial meniscus. At the nanoscale level, most of the tissue exhibited a well-oriented and fibrillar organization (Fig. 8 cp and YM images). Amorphous regions were confined to the W–W zone, and were also visible in SEM images, particularly between some pores. The lateral meniscus of P7 revealed a primarily amorphous and less organized nanostructure, with evident agglomerates and a heterogeneous stiffness (Fig. 9 cp and YM images). Microscopically, the morphology closely resembled that of the medial counterpart, exhibiting larger pores in the R-R zone and a more compact structure in the W-W region (Fig. 9 SEM images). The external portion showed a GAG distribution similar to the previous sample, although mucins were barely present in the inner region (Fig. 9

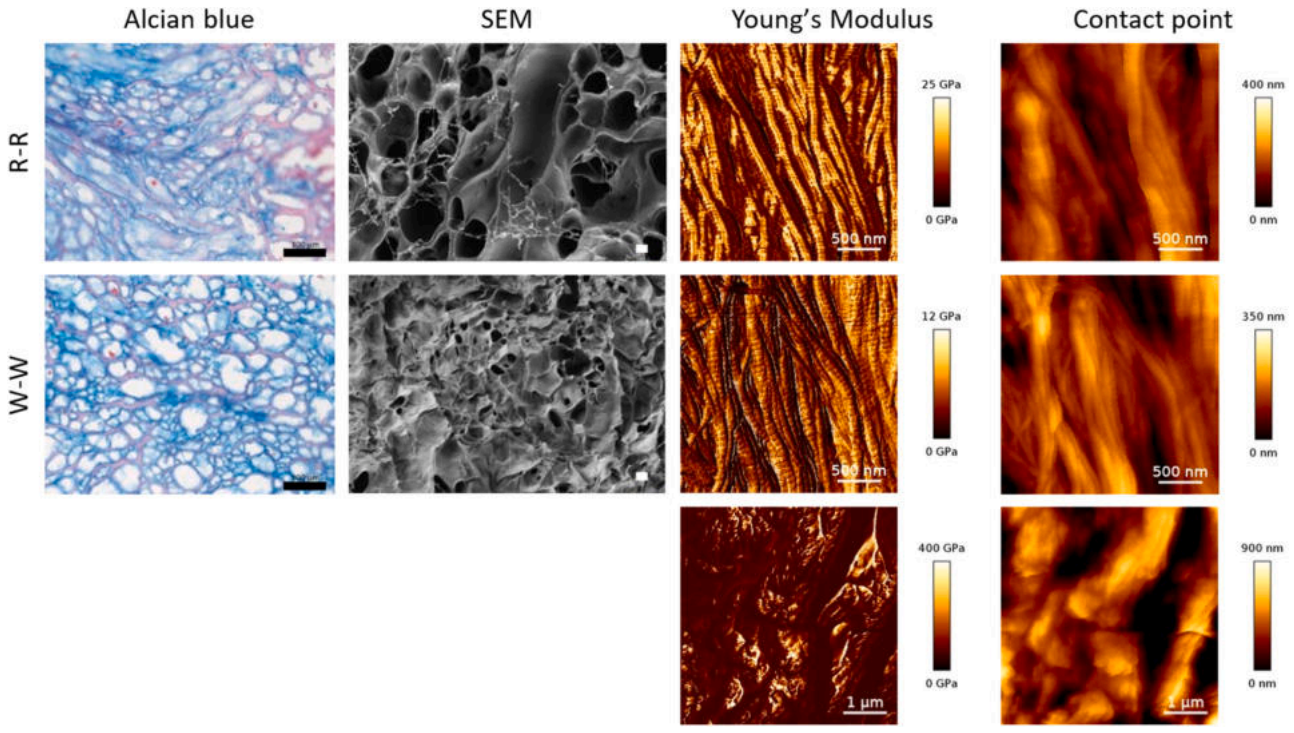

Fig. 8. Alcian blue staining, SEM and AFM images of YM and contact point acquired on P7 medial meniscal tissue. For W-W zone, two images were acquired due to the heterogeneous compostion of the ECM in this portion. Scale bars: 100 μm for Alcian blue images, 10 μm for SEM images, 500 nm for cp and YM images.

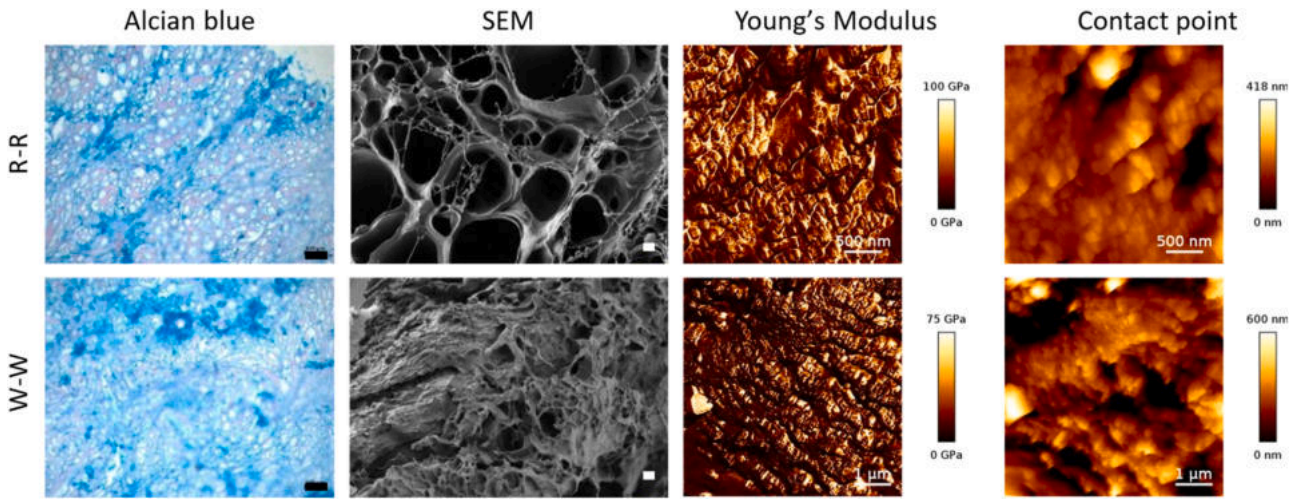

Fig. 9. Alcian blue staining, SEM and AFM images of YM and contact point acquired on P7 lateral meniscal tissue. Scale bars: 100 µm for Alcian blue images, 10 µm for SEM images, 500 nm for cp and YM images.

Alcian blue images). The medial meniscus of patient P8 demonstrated the greatest heterogeneity within the W–W zone. SEM analysis highlighted a complex and irregular matrix, which was also found nanoscopically in AFM imaging. These images revealed an intricate composition featuring fibrillar, porous, and amorphous regions (Fig. 10 cp and YM images). Greater structural regularity was observed in the outer zone, which resembled that of previous samples: porous at the microscopic level and amorphous at the nanoscale. The matrix contained an abundant number of mucins both internally and externally, although GAGs appeared to be more concentrated in the W-W zone (Fig. 10 Alcian blue images). In the lateral meniscus of P8, distinct differences between the outer and inner portions were also noted.

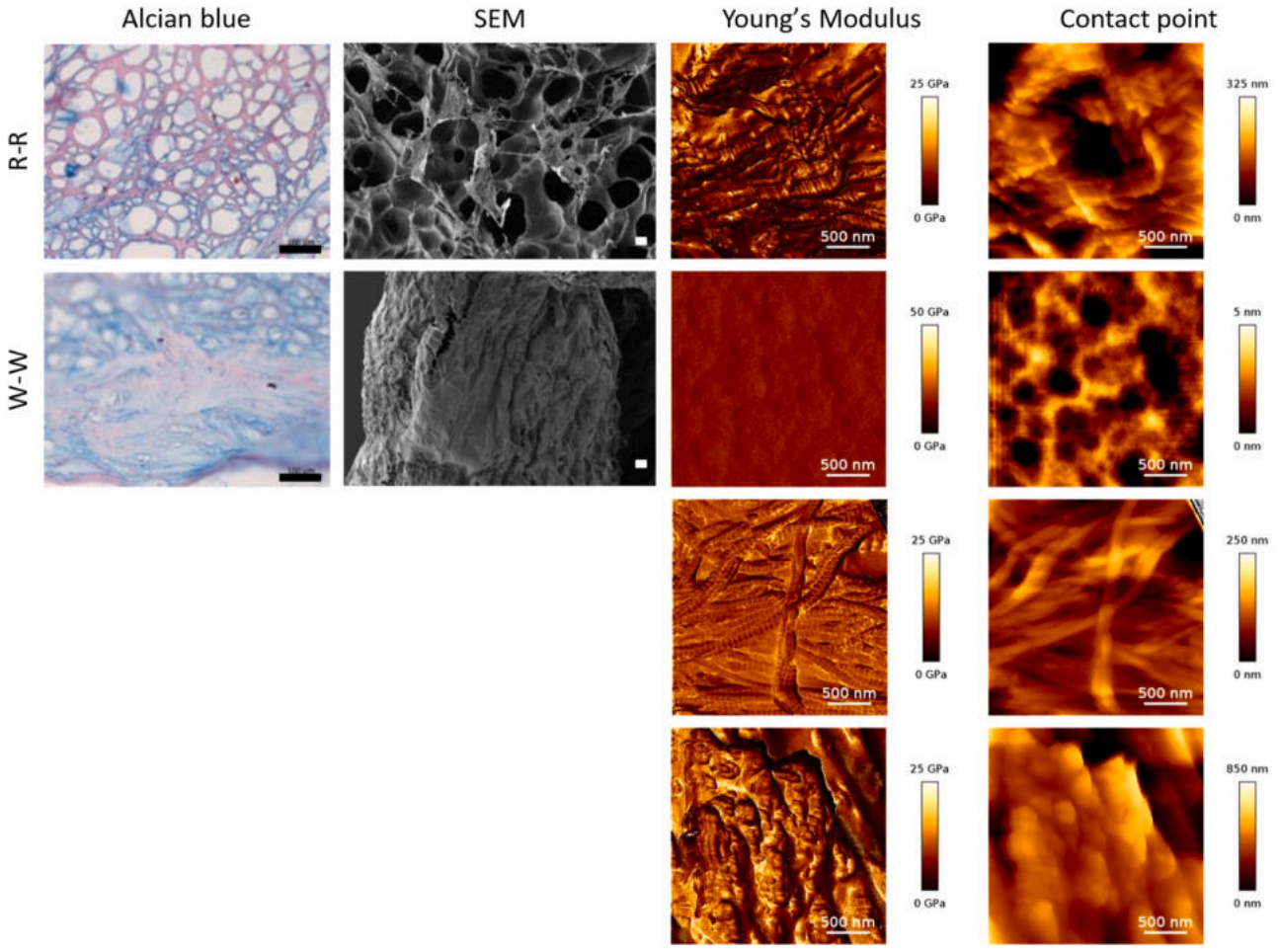

Fig. 10. Alcian blue staining, SEM and AFM images of YM and contact point acquired on P8 medial meniscal tissue. For W-W zone, three images were acquired due to the heterogeneous compostion of the ECM in this portion. Scale bars: 100 µm for Alcian blue images, 10 µm for SEM images, 500 nm for cp and YM images.

Macroscopically, the outer region appeared porous and well-organized, while the inner region was fibrous and more compact (Fig. 11 SEM images). The distribution of GAGs was similar to that observed in P6 lateral, with mucins abundantly present in both internal and external regions (Fig. 11 Alcian blue images). AFM analysis revealed subtle variations in nanostructure, with fibrillar elements present in the R–R zone, and a more porous and less organized composition deeper within the tissue (Fig. 11 cp and YM images).

In Fig. 12 the median values of YM obtained in R-R and W-W zones of meniscal tissue are shown. It is important to note that these YM values reflect nanoscale measurements, representing the stiffness of specific structural features or tissue organizations, such as localized fibrotic regions or characteristic collagen fibril orientations. The global compressive properties of meniscal tissue are described in the following paragraph. In P6, statistically significant differences in nanoscale stiffness were observed between lateral and medial menisci and between the R-R and W-W zones. Specifically, YM measured at the nanoscale was higher in the R-R portion of the lateral meniscus and lower in the corresponding medial region, suggesting more localized degeneration on the medial side. In contrast, nanoscale YM values in the W-W zones were comparable between lateral and medial menisci.

In P7 and P8, no statistically significant zonal differences were detected, suggesting a more globally distributed degeneration pattern. This lack of contrast between zones, compared to P6, could suggest a more generalized tissue degeneration rather than a localized degeneration. Nanoscale YM of the R-R zone in P7 was measured as slightly higher in the lateral side compared to the medial one, while a reduction was also visible in the W-W portions. Lateral nanoscale YM values in P8 were lower than medial ones, particularly in the lateral R-R zone. These findings are presented as case-specific observations within sample set and Mann-Whitney U test was chosen as conservative and distribution-free approach to identify measurable differences between specific regions, rather than to establish a generalized factorial model of aging or alignment. A global comparison of nanoscale YM across different formulations is shown in Figure S11 Supplementary Material.

3.5. Compression test

To assess global mechanical properties, meniscal tissue from patients P6, P7, and P8 underwent compression test up to 40 % deformation, from which YM was determined in the elastic region of the stress–strain curves (Fig. 13A). All curves displayed an initial toe region, characterized by a nonlinear stress-strain response with progressively increasing slope. This behaviour, typical of biological tissues, reflects the gradual realignment of wavy collagen fibres. Once the collagen fibrils became fully straightened, the elastic region began, where stress and strain showed a linear relationship and the slope corresponded to the YM [29]. In P6 and P7, the slope was similar in the lateral menisci and in the medial R-R zones, whereas the medial W-W zones exhibited slopes of greater magnitude. In contrast, in P8 the slopes were comparable across both W-W and R-R portions. It is important to note that at 40 % strain none of the samples reached the yield point, indicating that they remained within the elastic region.

YM values were calculated for each region in each sample, and statistical differences were evaluated using ANOVA with multiple comparisons (Fig. 13B and Table S1 Supplementary Material). Overall, YM was consistently higher in the W-W portions, consistent with collagen fibre orientation. In the R-R zones, collagen fibres are primarily aligned circumferentially, exposing their cross-sections under compression; these fibrils are optimized for tensile rather than compressive loading and therefore result in a less compact and more porous structure. Conversely, in the W-W zones, fibres exhibit a more random orientation, generating a denser matrix, as also confirmed by previous SEM observations, and yielding higher YM values. In agreement with previous results, P6 and P7 showed a marked decrease in YM in the lateral W-W zones, indicating localized deformation. Both patients exhibited valgus knee alignment, which increases loading on the lateral meniscus. This region is anatomically less stabilized by ligaments than the medial side, making it more susceptible to degeneration. Previous observations revealed a reduction in collagen fibres in these samples, which was not seen in the lateral W-W zone of P8. Since collagen fibres provide mechanical strength to the meniscal ECM, their loss due to degeneration

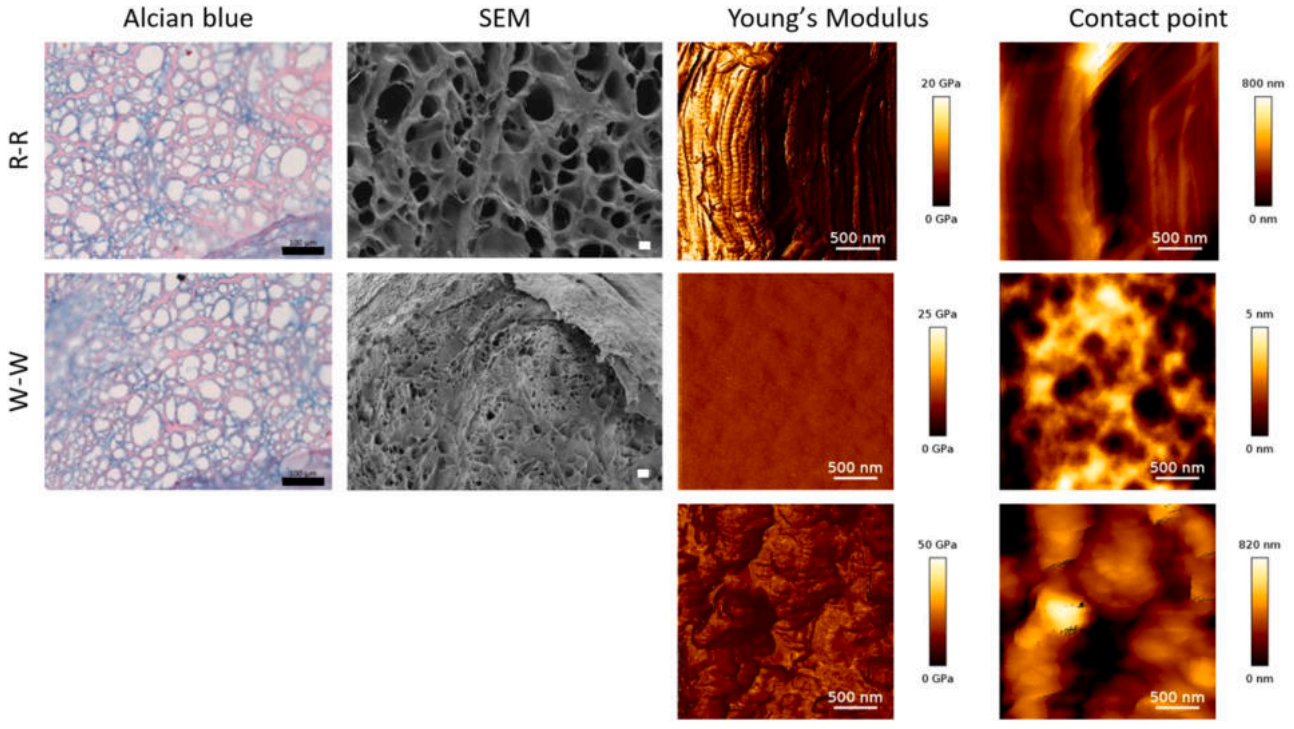

Fig. 11. Alcian blue staining, SEM and AFM images of YM and contact point acquired on P8 lateral meniscal tissue. For W-W zone, two images were acquired due to the heterogeneous compostion of the ECM in this portion. Scale bars: 100 μm for Alcian blue images, 10 μm for SEM images, 500 nm for cp and YM images.

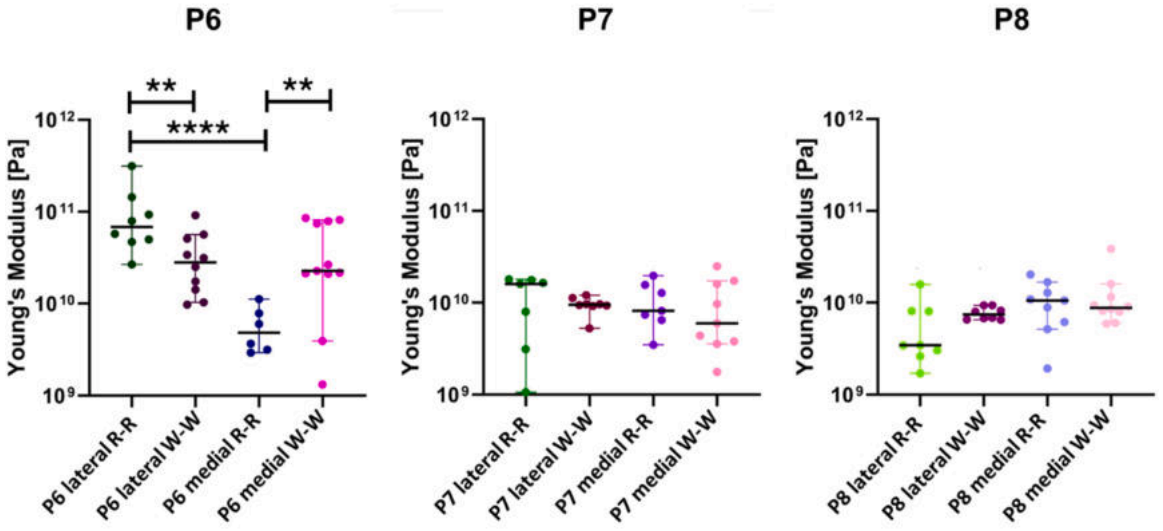

Fig. 12. median values of the AFM-derived mechanical parameters are shown for each region. Error bars represent the 95 % confidence intervals (95 % CI) calculated for each dataset. Pairwise statistical comparisons were performed using the Mann–Whitney U test and significative differences were shown with "*", where ** indicates $p < 0.05$, *** $p < 0.005$ and **** $p < 0.0005$.

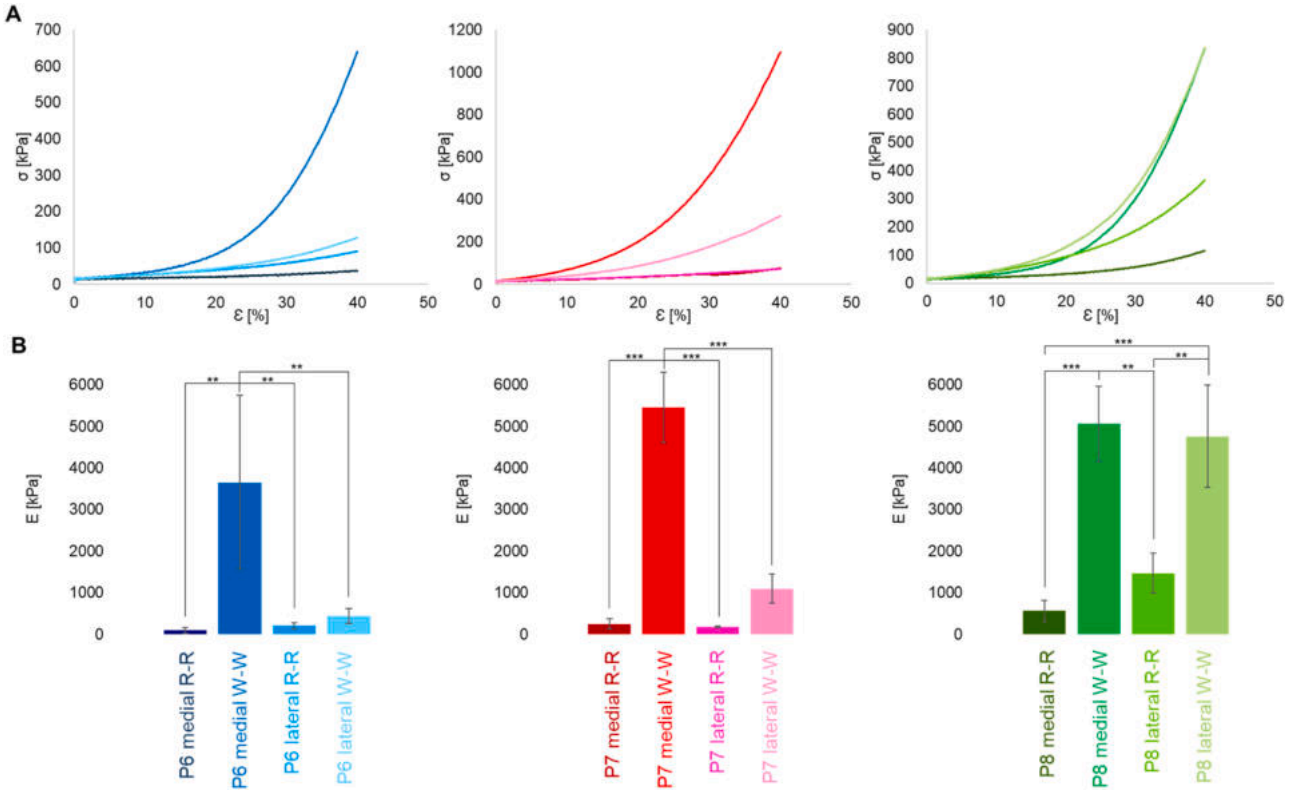

Fig. 13. stress-strain curves (A) and barplot showing YM values obtained from compression tests on meniscal tissue (B), where each bar represents the mean ± SD of three technical replicates per sample. Normality of each group was verified using the Shapiro-Wilk test. One-way ANOVA was used as the main statistical test, followed by Tukey's post-hoc test for multiple pairwise comparisons. Significative differences were indicated as"*" for $0.05<p \leq 0.001$, "**" for $0.01<p \leq 0.001$ and "***" for $p > 0.001$.

results in decreased mechanical properties. When comparing medial W-W zones, P7 and P8 exhibited similar YM values, whereas P6 displayed lower values. Given that P6 was the oldest patient, while P7 and P8 were of similar age, the reduction in YM in P6 likely reflects age-related degenerative changes. A similar trend was observed between P6 and P7: the younger patient had higher YM in the lateral W-W zone, implying that although valgus configuration is the main driver of reduction, aging likely amplifies the effect.

Differences were observed between YM values measured by AFM and those obtained from compression tests. This is consistent with the fact that compression testing reflects the macroscopic mechanical properties of the tissue, whereas AFM captures the YM of nanoscale structures,

which exhibit high heterogeneity due to the anisotropic nature of meniscal tissue. This heterogeneity arises from variations in collagen fibre orientation, as revealed by SEM, and differences in chemical composition between physiological and pathological regions, as shown by histological analysis.

4. Discussion

The menisci are essential in both tibiofemoral compartments for load distribution and shock absorption [18]. Different studies were performed to characterize meniscal ECM of different species from histological, morphological and biomechanical point of views, and several works compare them with human tissue (Table 5). In Sandmann et al., human meniscal tissue was compared with bovine, ovine, and porcine menisci from biomechanical and biochemical point of views to investigate species differences and identify the most physiologically similar tissue [16]. It is important to note that differences between human and animal ECM arise not only from variations in meniscal size but also from differences in knee flexion and extension during walking [15,16]. Moreover, both intra- and interspecies differences in meniscal tissue characteristics are well documented, as degeneration leads to macroscopic and microscopic alterations in the tissue [17]. The aim of this work was to evaluate the properties of meniscal ECM in human patients of different ages and with various pathologies, in order to study the changes associated with disease. Paediatric patients were also included, since their meniscal tissue, originating from traumatic rather than degenerative lesions, can be considered physiological. A comparison was also performed between lateral and medial menisci from normal and valgus knee to detect the ECM variations induced by this pathological state, in which knee joint is angled out and away from the body's mid-line [30].

4.1. Histological characterization

To study the histology of meniscal tissue, different stains were used: Haematoxylin-Eosin and Van Gieson Trichrome to evaluate the cellularity and Masson Trichrome, Alcian Blue and Safranin-Fast Green for the extracellular matrix characterization. In terms of cell morphology, two main cell types are present in meniscal tissue: fusiform fibroblast-like cells in the fibrocartilaginous region, which is subjected to tensile loads, and spherical chondrocyte-like cells in the inner region, which experiences compressive loads [15,31,32]. Overall, cell density is limited, and a slight decrease in the cell population is observed during meniscal degeneration. These observations are consistent with our H&E and Van Gieson staining results, which allowed visualization of cell nuclei and revealed occasional elongation of cells in regions corresponding to the fibrocartilaginous zone. Several studies on human meniscal tissue described a reduction in cell density, associated by mucoid degeneration and a loss of collagen fibre organization in pathological tissues, as well as age increases [11,18,33]. Concerning the ECM characterization, the content of collagen fibres stained with Masson Trichrome decreases in relation to the degeneration of the tissue (Figure S1 Supplementary material). A reduction in collagen content was observed in adult samples compared with paediatric samples. Paediatric samples exhibited similar collagen levels among themselves, while adult samples showed variability associated with both age and pathological condition. Further studies with larger cohorts are needed to disentangle the relative contributions of age and pathology. This result is consistent with Sun et al. study, where a decrease in collagen content in osteoarthritic patients using Picrosirius Red, a staining method analogous to Masson's trichrome for collagen detection [34]. Safranin O staining was performed with a Fast green counterstain to detect negatively charged proteoglycans, as it stoichiometrically binds to the anionic glycosaminoglycan component of proteoglycans [35,36]. In paediatric patients, proteoglycans were predominantly localized in the inner zone of the meniscus. In contrast, adult samples showed a more heterogeneous distribution: in some cases, proteoglycans were distributed throughout the entire section, whereas in others a reduced proteoglycan content was observed (Figure S2, Supplementary Material). Notably, the patient exhibiting the most pronounced collagen reduction also showed the strongest red staining, indicative of increased proteoglycan content. However, considerable variability was observed among the remaining patients, independently of age and pathological condition. These results align with previous works found in literature. For instance, in a Sun et al. study a comparison between normal and osteoarthritic menisci was done using Safranin O staining and an increase of proteoglycans was observed [37]. Similarly, Videman et al. reported a comparable result after inducing osteoarthritis through limb immobilization in rabbits [38]. However, Djurasovic et al. found a decrease in proteoglycan content following osteoarthrosis induction via limb immobilization in mature beagles [39]. Additionally, other studies have reported a reduction in proteoglycans in human osteoarthritic cartilage, highlighting the need for further research to better understand this phenomenon [40–42]. Alcian Blue staining was used to detect sulfated GAGs, which account for approximately 80 % of total GAGs. Paediatric samples exhibited markedly intense staining compared with pathological samples, in which an increase in mucins was observed (Figure S3, Supplementary Material). In adult patients, a reduction in sulfated GAG content was observed in some cases, appearing to be more closely associated with aging than with pathological condition. Ribitsch et al. studied meniscal tissues from horses of different ages and concluded that GAG content and distribution are age dependent. In young horses, GAGs were generally more evenly distributed, while in older horses, the menisci exhibited distinct areas of positive or negative GAG presence [21]. Lopez-Franco et al. investigated proteoglycans changes in human menisci and found a decrease in the matrix of osteoarthritic patients: consistently with other studies, GAGs synthesis is reduced during degeneration [11,43]. These results are consistent with Herwig et al. studies, in which alterations in water, collagen and GAGs content were observed in various degrees of degeneration [9]. Under the same physiological and biomechanical conditions, a decrease in collagen, GAGs, and ligamentous tissue, along with an increase in mucins, can be observed in the medial meniscus (Figure S6, S7 and S8 Supplementary material): this result aligns with the fact that the medial compartment is more congruent than the lateral compartment, making it more susceptible to increased compression and more frequent meniscal tears [24,

Table 5
Characteristics of meniscal tissue in human and animals.

Source	Results	References
Human paediatric	Collagen predominant in the outer zone, GAGs in the inner zone, low cellularity. Ligamentous-like structure in the external part, cartilaginous-like in the internal one. Collagen fibres are physiologically oriented and no damaged.	This study
Human adult	Collagen and GAGs decrease when age increases, mucins and fibrotic tissue increase. Low cellularity. Collagen fibres are more irregular and thicker. At nanoscale level, great heterogeneity of the tissue, varying from porous to fibrillar and amorphous aspect.	This study
Human	In pathological meniscal tissue, matrix degeneration and different biochemical properties are observed.	[15,16, 18]
Bovine	Fibres organization and thickness increase with age due to higher loading.	[19]
Ovine	Is the most like the human meniscus from viscoelastic and biological point of views. Collagen pattern is consistent with human tissue.	[15,16]
Pig	GAGs distribution is different, but collagen fibre's structure is like human meniscus.	[16,20]
Horse	GAGs content and distribution is age-dependant, like in human meniscal tissue.	[21]
Rabbit	Different biomechanics to human meniscal tissue, cellularity and vascularization are higher. Collagen pattern is consistent with human tissue.	[15,16]

44]. In the case of a valgus knee, greater degeneration is observed in the ECM of the lateral meniscus. This is attributed to alterations in the joint biomechanics, leading to increased damage and erosion on the lateral side [45,46].

From a biochemical perspective, ECM homeostasis is maintained by a balance between anabolic processes and catabolic activity mediated by enzymes such as MMP-13 and ADAMTS-5, which are counteracted by inhibitors including TIMP-1. Although we did not directly measure these catabolic mediators, it is plausible that the ECM remodelling observed here results from a combination of decreased matrix synthesis and increased degradation, as described in similar tissues [47–49]. Future studies including the assessment of ECM-degrading enzymes and their inhibitors will be essential to clarify the relative contribution of these mechanisms.

4.2. Morphological characterization

Morphologically, three distinct layers were observed in all samples: a thin fibrillar network covering the femoral and tibial surfaces, a radially oriented lamellar layer, and a central region characterized by circumferentially aligned fibres. This hierarchical fibre organization is closely related to meniscal function in load transmission and distribution. Under compressive load from the femur, circumferential fibres elongate and convert compressive forces into tensile stresses, thereby facilitating load redistribution, while radial fibres contribute to maintaining structural integrity by constraining the tissue architecture. This collagen orientation has been widely reported in the literature. For instance, Petersen et al. described a randomly oriented superficial fibrillar layer with fibril diameters of approximately 35 nm, underlain by collagen fibrils of about 120 nm in diameter, forming a superficial layer approximately 150–200 μm thick. Notably, the thickness of this layer decreases to 20–30 μm toward the inner circumference [13].

Differences were observed in the rabbit meniscal ECM, where the lamellar layer was not detected, highlighting the importance of having significative data on humans [15]. In paediatric samples and in younger patients with traumatic injury, collagen fibres were thinner, smoother, and exhibited regular porosity in both the Red-Red and White-White zones. In contrast, degenerative conditions and aging were associated with thicker, irregular fibres and more heterogeneous pore structure, suggestive of fibrotic tissue, particularly in the medial meniscus. A similar structural pattern was observed in the lateral meniscus of valgus knees. While previous studies employing AFM have been employed to quantify meniscal micromechanics of animal or adult human tissues, they did not integrate pathological alignment conditions. In this work nanoscale stiffness have been integrated with histological and microstructural features in rare human specimens. In detail, nanoscale imaging using QI-mode AFM further confirmed the heterogeneous ECM composition, encompassing porous, fibrillar, and amorphous regions, thereby highlighting the intrinsic anisotropy of meniscal tissue. Similar fibrils with a comparable diameter were observed in previous works on murine and porcine meniscal tissues [50,51]. When comparing different biomechanical configurations, patient with valgus alignment combined with aging exhibited drastically reduced localized stiffness in the R-R zone of the medial meniscus, suggesting signs of degeneration. Statistically significant differences in stiffness among the various meniscal zones were observed in this group, indicating a clear distinction between regions. Conversely, in P7 and P8, which both had normal and valgus alignment, localized YM of the R-R and W-W zones of both medial and lateral menisci did not show statistically significant differences. This reduced contrast between zones may be attributed to more generalized tissue degeneration, less localized within the medial meniscus R-R zone. This interpretation is supported by the markedly decreased stiffness values observed in the R-R zones of the lateral meniscus in these patients. Additionally, the W-W zones demonstrated localized stiffness more comparable to those of the normal knee. In Kwok et al., nanomechanical profiles of meniscal tissues from healthy young, aged and osteoarthritic patients were evaluated using AFM. Healthy aged tissue showed similar differential elasticity among inner and outer zones, with higher YM externally, instead degenerated osteoarthritic tissue showed more similar stiffness in R-R and W-W zones [52].

From the biochemical point of view, all samples presented mucoid degeneration, which seemed to be more evident in lateral menisci, which is also associated to loss of collagen fibre organization. These results align with a previous study in which Alcian Blue and Safranin O staining were quantified to analyse human meniscal tissues from patients of varying ages and pathological conditions, aiming to identify ECM changes associated with age and disease. That study reported a decrease in cell density and an increase in mucoid degeneration, which correlated with a loss of collagen fibre organization as pathology progressed. Moreover, pathological samples exhibited heterogeneous proteoglycan distribution, with regions of intense staining alongside areas lacking any signal. These observations are consistent with the data obtained in the present work [18].

4.3. Mechanical characterization

Global compressive properties of meniscal cross-sections were also assessed, revealing lower YM in R-R zones, consistent with the predominance of circumferential collagen fibres in this region, which primarily function under tension rather than compression. In W-W zones, patients with valgus knee alignment exhibited a marked reduction in YM in the lateral compartment, reflecting greater degeneration due to altered biomechanical loading; this was accompanied by decreased collagen content, as confirmed by histological analysis. Furthermore, a gradual decline in YM with age was observed in W-W zones of medial menisci, indicating that aging contributes to the progressive deterioration of tissue mechanical properties. In Fischenich et al., the mechanical properties of human menisci at different stages of osteoarthritic damage were examined. Their results indicated that tensile YM remained unchanged across all degenerative grades, while compressive YM was already affected in the early stages of gross degeneration and continued to decline with disease progression, consistent with our observations [53]. Assessing compressive YM in patients is therefore clinically relevant, as it may serve as a valuable indicator to guide surgical decisions, such as whether to resect or suture a meniscal tear [54]. This underscores the importance of our study, in which we also linked pathological biochemical alterations to changes in compressive YM.

5. Limits and perspectives

This study is subject to several limitations. One could be the small sample size, which included only eight patients, making it difficult to draw generalizable conclusions. To our knowledge, this research represents the first attempt to characterize the "meniscal ECM" in skeletally immature subjects [55].

Although a significant increase in meniscal procedures in children has been documented, the difficulties in increasing the number of samples are evident. In fact, in our routine clinical practice, most patients programmed for meniscal pathologies are treated with meniscal repair and suture surgery [56]. Consequently, these samples were not used for inferential statistical comparisons but were included to provide to our knowledge the first descriptive insights on physiological human meniscal ECM. Additionally, no previous studies have specifically examined the correlation between physical properties of the meniscal ECM, such as stiffness, and the tissue morphology and histological composition in both healthy and pathological menisci. This study evaluated the impact of various pathologies, including valgus knee alignment and arthritis, on tissue morphology, stiffness, and composition, as well as the interrelationships among these factors. Moreover, the fact that this is a single-centre study may further limit generalizability, as all data were collected from a single hospital, potentially restricting its applicability to broader clinical settings. Variability in the sampling

technique is another limitation, differences in surgical methods (e.g., en bloc meniscectomy) and the exclusion of smaller meniscal tears could introduce selection bias by including only specific types of lesions. Furthermore, the exclusive use of discarded tissue from surgery may not fully represent the entire meniscus or its different zones comprehensively. For this reason, future directions include expanding the study to additional meniscal samples from various lesion types and anatomical regions to gain a deeper understanding of ECM degeneration processes and to obtain more generalizable results. A further limitation is that sex and hormonal variables were not systematically matched or controlled. Estrogen is known to influence collagen cross-linking and glycosaminoglycan (GAG) synthesis, which may affect the studied outcomes; therefore, these factors should be carefully controlled in future studies with larger cohorts. However, the results observed in both paediatric and adult pathological meniscal tissues are consistent with findings reported in a previous study [18], supporting the reliability of the data. With the integration of histological, ultrastructural, and multiscale mechanical analyses, this study provides for the first time an engineering-oriented characterization of human meniscal tissue fundamental to evaluate the principal key properties to replicate in the design of meniscal substitute and tissue engineered constructs. The combined evaluation of ECM microstructure, the general biomolecular composition and the evaluation of stiffness offers parameters that are relevant for biomechanical modelling, scaffold design, and regenerative strategies. Specifically, the structural and biochemical alterations described in the literature were also identified in this work. However, no prior data were available comparing valgus knee alignment to physiological and paediatric conditions. This study is particularly significant as it is the first to examine the correlation between morphology, histological composition, and stiffness in meniscal tissue across patients of varying ages and with different pathologies. The results obtained may be significant not only for improving the medical diagnosis of meniscal pathologies but also for the development of personalized treatments, given that each meniscal condition presents unique ECM differences in both stiffness and composition. Following this multi-characterization approach, this work can be useful in regenerative medicine, as the design of a functional scaffold must replicate both the mechanical and biochemical properties of native tissue.

Ethical approval

Study approved by the local Ethical Committee (Comitato Etico, Fondazione San Gerardo dei Tintori, Italy), Bioknee Protocol n. 0013,842 (04/05/2023), act n. 571 (21/11/2023), written informed consent was obtained from all patients and healthy subjects before they entered the study, performed in accordance with the Declaration of Helsinki.

CRediT authorship contribution statement

Maddalena Bracchi: Writing – original draft, Validation, Methodology, Investigation, Formal analysis, Data curation. **Riccardo Campanile:** Writing – original draft, Validation, Methodology, Investigation, Formal analysis, Data curation. **Marco Crippa:** Writing – review & editing, Resources. **Mario Mauri:** Methodology, Data curation. **Valeria Cassina:** Writing – review & editing, Supervision. **Francesco Mantegazza:** Writing – review & editing, Supervision. **Francesco Nicotra:** Writing – review & editing, Supervision, Funding acquisition. **Judith Waldner:** Writing – review & editing, Resources. **Giovanni Zatti:** Writing – review & editing, Resources. **Marco Bigoni:** Writing – review & editing, Resources. **Marco Turati:** Writing – review & editing, Supervision, Project administration. **Laura Russo:** Writing – review & editing, Supervision, Project administration, Funding acquisition.

Declaration of competing interest

The authors declare that they have no known competing financial interests or personal relationships that could have appeared to influence the work reported in this paper.

Acknowledgements

Supported by a grant from Italian Ministry for Universities and Research (MUR), Dipartimenti di Eccellenza 2023–2027 (l. 232/2016, art. 1, commi 314–337). Financial support from: Iniziativa "PNC0000003 - "ANTHEM: AdvaNced Technologies for Human-centrEd Medicine". CUP BICOCCA B53C2200667000..

Supplementary materials

Supplementary material associated with this article can be found, in the online version, at doi:10.1016/j.rineng.2026.110058.

Data availability

Data will be made available on request.

References

[1] A. Aazmi, et al., Biofabrication methods for reconstructing extracellular matrix mimetics, Bioact. Mater. 31 (Jan. 2024) 475–496, https://doi.org/10.1016/j.bioactmat.2023.08.018.
[2] J. Nicolas, S. Magli, L. Rabbachin, S. Sampaolesi, F. Nicotra, L. Russo, 3D Extracellular matrix mimics: fundamental concepts and role of materials chemistry to influence stem cell fate, Biomacromolecules 21 (6) (Jun. 2020) 1968–1994, https://doi.org/10.1021/acs.biomac.0c00045.
[3] S. Zhu, et al., Microstructure analysis and reconstruction of a meniscus, Orthop. Surg. 13 (1) (Feb. 2021) 306–313, https://doi.org/10.1111/os.12899.
[4] E. Luvsannyam, M.S. Jain, A.R. Leitao, N. Maikawa, A.E. Leitao, Meniscus tear: pathology, incidence, and management, Cureus (May 2022), https://doi.org/10.7759/cureus.25121.
[5] E.A. Makris, P. Hadidi, and K.A. Athanasiou, "The knee meniscus: structure-function, pathophysiology, current repair techniques, and prospects for regeneration," Oct. 2011. doi: 10.1016/j.biomaterials.2011.06.037.
[6] P.E. Gelber, B. Barenius, S. Perelli, Role of alignment and osteotomy in meniscal injuries, W.B.Saunders, Jan. 01, 2020, https://doi.org/10.1016/j.csm.2019.08.006.
[7] M. López-Franco, E. Gómez-Barrena, Cellular and molecular meniscal changes in the degenerative knee: a review, Springer, 2018, https://doi.org/10.1186/s40634-018-0126-8.
[8] C.S. Proctor, M.B. Schmidt, R.R. Whipple, M.A. Kelly, and V.C. Mow, "Material properties of the normal medial Bovine Meniscus," 1989. doi: 10.1002/jor.1100070602.
[9] J. Herwig, E. Egner, and E. Buddecke, "Chemical changes of human knee joint menisci in various stages of degeneration," Aug. 1984. doi: 10.1136/ard.43.4.635.
[10] C.A. Mcdevitt and R.J. Webber, "The ultrastructure and biochemistry of meniscal cartilage," Mar. 1990. do i: PMID:2406077.
[11] M. López-Franco, et al., Meniscal degeneration in human knee osteoarthritis: in situ hybridization and immunohistochemistry study, Arch. Orthop. Trauma Surg. 136 (2) (Feb. 2016) 175–183, https://doi.org/10.1007/s00402-015-2378-4.
[12] F. Flandry and G. Hommel, "Normal anatomy and biomechanics of the knee," Jun. 2011. doi: 10.1097/JSA.0b013e318210c0aa.
[13] W. Petersen, B. Tillmann, Collagenous fibril texture of the human knee joint menisci, Anat. Embryol. (Berl) 197 (4) (Mar. 1998) 317–324, https://doi.org/10.1007/s004290050141.
[14] E. Stocco, A. Porzionato, E. De Rose, S. Barbon, R. De Caro, V. Macchi, Meniscus regeneration by 3D printing technologies: current advances and future perspectives, SAGE Publications Ltd, Jan. 01, 2022, https://doi.org/10.1177/20417314211065860.
[15] A. Chevrier, M. Nelea, M.B. Hurtig, C.D. Hoemann, M.D. Buschmann, Meniscus structure in human, sheep, and rabbit for animal models of meniscus repair, J. Orthopaed. Res. 27 (9) (Sep. 2009) 1197–1203, https://doi.org/10.1002/jor.20869.
[16] G.H. Sandmann, et al., Biomechanical comparison of menisci from different species and artificial constructs, BMC Musculoskelet. Disord. 14 (2013), https://doi.org/10.1186/1471-2474-14-324.
[17] M.A. Sweigart et al., "Intraspecies and interspecies comparison of the compressive properties of the Medial Meniscus," Nov. 2004. doi: 10.1114/b:abme.0000049040.70767.5c.
[18] C. Pauli, et al., MAcroscopic and histopathologic analysis of Human knee menisci In aging and osteoarthritis, Osteoarthr. Cartil. 19 (9) (Sep. 2011) 1132–1141, https://doi.org/10.1016/j.joca.2011.05.008.

[19] S. Bansal, et al., Structure, function, and defect tolerance with maturation of the radial tie fiber network in the knee meniscus, J. Orthop. Res. 38 (12) (Dec. 2020) 2709–2720, https://doi.org/10.1002/jor.24697.
[20] Y. He, et al., Preparation and characterization of an optimized meniscal extracellular matrix scaffold for Meniscus transplantation, Front. Bioeng. Biotechnol. 8 (Jul. 2020), https://doi.org/10.3389/fbioe.2020.00779.
[21] I. Ribitsch, et al., Structure—Function relationships of equine menisci, PLoS One 13 (3) (Mar. 2018), https://doi.org/10.1371/journal.pone.0194052.
[22] K. Nakagawa, et al., Histological analysis of the wrapping treatment for meniscal horizontal tears in rabbits, Cartilage 13 (2_suppl) (Dec. 2021) 1551S–1561S, https://doi.org/10.1177/1947603519870838.
[23] P.E. Greis, D.D. Bardana, M.C. Holmstrom, and R.T. Burks, "Meniscal injury: I. Basic science and evaluation.," 2002. doi: 10.5435/00124635-200205000-00003.
[24] M. Englund, A. Guermazi, and L.S. Lohmander, "The meniscus in knee osteoarthritis," Aug. 2009. doi: 10.1016/j.rdc.2009.08.004.
[25] M. Sampietro, et al., The nanomechanical properties of CLL cells are linked to the actin cytoskeleton and are a potential target of BTK inhibitors, Hemasphere 7 (8) (Aug. 2023) e931, https://doi.org/10.1097/HS9.0000000000000931.
[26] M.J. Higgins, et al., Noninvasive determination of optical lever sensitivity in atomic force microscopy, Rev. Sci. Instrum. 77 (1) (Jan. 2006), https://doi.org/10.1063/1.2162455.
[27] H. Schillers, et al., Standardized nanomechanical atomic force microscopy procedure (SNAP) for measuring soft and biological samples, Sci. Rep. 7 (1) (Jul. 2017) 5117, https://doi.org/10.1038/s41598-017-05383-0.
[28] D. Wu, P. Isaksson, S.J. Ferguson, C. Persson, Young's modulus of trabecular bone at the tissue level: a review, Acta Biomater 78 (Sep. 2018) 1–12, https://doi.org/10.1016/j.actbio.2018.08.001.
[29] R. K. S. Saarakkal, Biomechanics and modeling of skeletal soft tissues. Theoretical biomechanics, InTech, 2011, https://doi.org/10.5772/19975.
[30] P. Ahsan, Md.S. Ezaz, I. Jahan, N.S. Asma, M. Anjoom, Total knee replacement in a young patient with valgus knee osteoarthritis: a case report, J. Orthop. Case Rep. 14 (1) (2024) 48–53, https://doi.org/10.13107/jocr.2024.v14.i01.4144.
[31] F.N. Ghadially, I. Thomas, N. Yong, and J.-M.A. Lalonde, "Ultrastructure of rabbit semilunar cartilages," 1978. do i: PMID:580431.
[32] M.-P. Hellio et al., "The cells of the rabbit meniscus : their arrangement, interrelationship, morphological variations and cytoarchitecture," May 2001. doi: 10.1046/j.1469-7580.2000.19850525.x.
[33] M. Albersheim, et al., Cell count and Cell density decrease as age increases in cadaveric pediatric medial menisci, Arthrosc. Sports Med. Rehabil. 5 (6) (Dec. 2023), https://doi.org/10.1016/j.asmr.2023.100795.
[34] V. MARCOS-GARCÉS, M. HARVAT, P. MOLINA AGUILAR, A. FERRÁNDEZ IZQUIERDO, A. RUIZ-SAURÍ, Comparative measurement of collagen bundle orientation by Fourier analysis and semiquantitative evaluation: reliability and agreement in Masson's trichrome, Picrosirius red and confocal microscopy techniques, J. Microsc. 267 (2) (Aug. 2017) 130–142, https://doi.org/10.1111/jmi.12553.
[35] A. Alibegović, R. Blagus, I.Z. Martinez, Safranin O without fast green is the best staining method for testing the degradation of macromolecules in a cartilage extracellular matrix for the determination of the postmortem interval, Forensic Sci. Med. Pathol. 16 (2) (Jun. 2020) 252–258, https://doi.org/10.1007/s12024-019-00208-0.
[36] K.M. Kjosness, P.L. Reno, M.A. Serrat, Modified periodic <scp>acid-schiff</scp>(<scp>PAS</scp>) is an alternative to Safranin O for discriminating bone–Cartilage interfaces, JBMR Plus 7 (6) (Jun. 2023), https://doi.org/10.1002/jbm4.10742.
[37] Y. Sun, et al., Histological examination of collagen and proteoglycan changes in osteoarthritic menisci, Open Rheumatol. J. 6 (2012) 24–32, https://doi.org/10.2174/1874312901206010024.
[38] T. Videman, I. Eronen, C. Friman, A. Langenskiöld, Glycosaminoglycan metabolism of the medial meniscus, the medial collateral ligament and the hip joint capsule in experimental osteoarthritis caused by immobilization of the rabbit knee, Acta Orthop. Scand. 50 (4) (Jan. 1979) 465–470, https://doi.org/10.3109/17453677908989791.
[39] M. Djurasovic, J.W. Aldridge, R. Grumbles, M.P. Rosenwasser, D. Howell, A. Ratcliffe, Knee joint immobilization decreases aggrecan gene expression in the meniscus, Am. J. Sports Med. 26 (3) (May 1998) 460–466, https://doi.org/10.1177/03635465980260032101.
[40] S. Saarakkala, P. Julkunen, P. Kiviranta, J. Mäkitalo, J.S. Jurvelin, R.K. Korhonen, Depth-wise progression of osteoarthritis in human articular cartilage: investigation of composition, structure and biomechanics, Osteoarthr. Cartil. 18 (1) (Jan. 2010) 73–81, https://doi.org/10.1016/j.joca.2009.08.003.
[41] A. Lahm, et al., Changes in content and synthesis of collagen types and proteoglycans in osteoarthritis of the knee joint and comparison of quantitative analysis with Photoshop-based image analysis, Arch. Orthop. Trauma Surg. 130 (4) (Apr. 2010) 557–564, https://doi.org/10.1007/s00402-009-0981-y.
[42] G.R. Squires, S. Okouneff, M. Ionescu, A.R. Poole, The pathobiology of focal lesion development in aging human articular cartilage and molecular matrix changes characteristic of osteoarthritis, Arthritis Rheum. 48 (5) (May 2003) 1261–1270, https://doi.org/10.1002/art.10976.
[43] J.A. 'Buckwalter, H.J. 'Mankin, A.J. 'Grodzinsky, Articular cartilage and osteoarthrits, Instr Course Lect. 2005 54 (2005) 465–480. PMID:15952258.
[44] S.D. Masouros, I.D. McDermott, A.A. Amis, A.M.J. Bull, Biomechanics of the meniscus-meniscal ligament construct of the knee, Knee Surg. Sports Traumatol. Arthrosc. 16 (12) (Dec. 2008) 1121–1132, https://doi.org/10.1007/s00167-008-0616-9.
[45] P.E. Gelber, B. Barenius, S. Perelli, Role of alignment and osteotomy in meniscal injuries, Clin, Sports Med. 39 (1) (Jan. 2020) 211–221, https://doi.org/10.1016/j.csm.2019.08.006.
[46] D. Nikolopoulos, I. Michos, G. Safos, P. Safos, Current surgical strategies for total arthroplasty in valgus knee, World J. Orthop. 6 (6) (2015) 469, https://doi.org/10.5312/wjo.v6.i6.469.
[47] G.A. Cabral-Pacheco, et al., The roles of matrix metalloproteinases and their inhibitors in Human diseases, Int, J. Mol, Sci. 21 (24) (Dec. 2020) 9739, https://doi.org/10.3390/ijms21249739.
[48] E. Yalcinkaya, M. Celik, B. Bugan, Extracellular matrix turnover: a balance between MMPs and their inhibitors, Arq, Bras, Cardiol. (2014), https://doi.org/10.5935/abc.20140061.
[49] D.J. Leong, et al., Matrix metalloproteinase-3 in articular cartilage is upregulated by joint immobilization and suppressed by passive joint motion, Matrix Biol. 29 (5) (Jun. 2010) 420–426, https://doi.org/10.1016/j.matbio.2010.02.004.
[50] Q. Li, et al., Biomechanical properties of murine meniscus surface via AFM-based nanoindentation, J. Biomech. 48 (8) (Jun. 2015) 1364–1370, https://doi.org/10.1016/j.jbiomech.2015.02.064.
[51] J. Sanchez-Adams, R.E. Wilusz, F. Guilak, Atomic force microscopy reveals regional variations in the micromechanical properties of the pericellular and extracellular matrices of the meniscus, J. Orthop. Res. 31 (8) (Aug. 2013) 1218–1225, https://doi.org/10.1002/jor.22362.
[52] J. Kwok, S. Grogan, B. Meckes, F. Arce, R. Lal, D. D'Lima, Atomic force microscopy reveals age-dependent changes in nanomechanical properties of the extracellular matrix of native human menisci: implications for joint degeneration and osteoarthritis, Nanomedicine 10 (8) (Nov. 2014) 1777–1785, https://doi.org/10.1016/j.nano.2014.06.010.
[53] K.M. Fischenich, J. Lewis, K.A. Kindsfater, T.S. Bailey, T.L. Haut Donahue, Effects of degeneration on the compressive and tensile properties of human meniscus, J. Biomech. 48 (8) (Jun. 2015) 1407–1411, https://doi.org/10.1016/j.jbiomech.2015.02.042.
[54] B. Rasheed, et al., Intraoperative identification of patient-specific elastic modulus of the meniscus during arthroscopy, Comput. Methods Programs Biomed. 254 (Sep. 2024) 108269, https://doi.org/10.1016/j.cmpb.2024.108269.
[55] M. Turati, et al., An increase in paediatric arthroscopy in Europe: experience of the EPOS sport study group, J. Child, Orthop. 19 (1) (Feb. 2025) 64–74, https://doi.org/10.1177/18632521241302997.
[56] M. Hampton, F. Ali, N. Nicolaou, A. Ajuied, The management of isolated meniscal tears in skeletally immature children. An international expert consensus, Knee Surg. Sports Traumatol. Arthrosc. (Oct. 2024), https://doi.org/10.1002/ksa.12493.